SLAC-PUB-7489

June 1997

MEASUREMENT OF THE B HADRON ENERGY DISTRIBUTION IN Z^0 DECAYS*

The SLD Collaboration**

Stanford Linear Accelerator Center

Stanford University, Stanford, CA 94309

ABSTRACT

We have measured the B hadron energy distribution in Z^0 decays using a sample of semi-leptonic B decays recorded in the SLD experiment at SLAC. The energy of each tagged B hadron was reconstructed using information from the lepton and a partially-reconstructed charm-decay vertex. We compared the scaled energy distribution with several models of heavy quark fragmentation. The average scaled energy of primary B hadrons was found to be $< x_{E_B} >= 0.716 \pm 0.011(\text{stat.})\ ^{+0.021}_{-0.022}\ (\text{syst.})$.

Submitted to Physical Review D

Contributed to the XVIII International Symposium on Lepton Photon Interactions, July 28 - August 1 1997, Hamburg, Germany, and to the International Europhysics Conference on High Energy Physics, 19-26 August 1997, Jerusalem, Israel; Ref: 285.

1 Introduction

The production of heavy hadrons (H) in e^+e^- annihilation provides a laboratory for the study of heavy-quark (Q) jet fragmentation. This is commonly characterised in terms of the observable $x_{E_H} \equiv 2E_H/\sqrt{s}$, where E_H is the energy of a B or D hadron containing a b or c quark, respectively, and $\sqrt{s}$ is the c.m. energy. In contrast to light-quark jet fragmentation one expects [1] the distribution of x_{E_H}, $D(x_{E_H})$, to peak at an x_{E_H}-value significantly above 0. Since the hadronisation process is intrinsically non-perturbative $D(x_{E_H})$ cannot be calculated directly using perturbative Quantum Chromodynamics (QCD). However, the distribution of the closely-related variable $x_{E_Q} \equiv 2E_Q/\sqrt{s}$ can be calculated perturbatively [2, 3, 4] and related, via model-dependent assumptions, to the observable quantity $D(x_{E_H})$; a number of such models of heavy quark fragmentation have been proposed [5, 6, 7]. Measurements of $D(x_{E_H})$ thus serve to constrain both perturbative QCD and the model predictions. Furthermore, the measurement of $D(x_{E_H})$ at different c.m. energies can be used to test QCD evolution, and comparison of $D(x_{E_B})$ with $D(x_{E_D})$ can be used to test heavy quark symmetry [8]. Finally, the uncertainty on the forms of $D(x_{E_D})$ and $D(x_{E_B})$ must be taken into account in studies of the production and decay of heavy quarks, see *eg.* [9]; more accurate measurements of these forms will allow increased precision in tests of the electroweak heavy-quark sector.

Here we consider measurement of the B hadron scaled energy distribution $D(x_{E_B})$ in Z^0 decays. Earlier studies [10] used the momentum spectrum of the lepton from semi-leptonic B decays to constrain the mean value $< x_{E_B} >$ and found it to be approximately 0.70; this is in agreement with the results of similar studies at $\sqrt{s} = 29$ and 35 GeV [11]. In more recent analyses [12, 13] the scaled energy distribution $D(x_{E_B})$ has been measured by reconstructing B hadrons via their $B \rightarrow DlX$ decay mode; we have applied a similar technique. We used the precise SLD tracking system to select jets containing a $B \rightarrow DlX$ decay, where the charmed hadron D was identified semi-inclusively from a secondary decay vertex formed from charged tracks. Each hadronic vertex was then associated with a lepton l ($l = e$ or μ) with large momentum transverse to the jet direction. Neutral energy depositions measured in the hermetic calorimeter, as well as the energies of charged tracks, that were not associated with the Dl system were subtracted from the jet energy to yield the reconstructed B hadron energy. This measurement technique may be useful to B-lifetime or B-mixing analyses [14] where the proper time $t = L/\sqrt{\gamma^2 - 1}$, where $\gamma = E_B/m_B$, m_B is the B hadron mass and L is the decay length, must be known accurately. We then compared the B energy distribution with the perturbative QCD and phenomenological model predictions.

2 Apparatus and Hadronic Event Selection

The e^+e^- annihilation events produced at the Z^0 resonance by the SLAC Linear Collider (SLC) were recorded using the SLC Large Detector (SLD). A general description of the SLD can be found elsewhere [15]. This analysis used charged tracks measured in the Central Drift Chamber (CDC) [16] and in the Vertex Detector (VXD) [17], energy clusters measured in the Liquid Argon Calorimeter (LAC) [18], and muons measured in the Warm Iron Calorimeter (WIC) [19]. Electron identification utilizes CDC tracks and LAC clusters [20].

Momentum measurement is provided by a uniform axial magnetic field of 0.6 T. The CDC and VXD give a momentum resolution of $\sigma_{p_\perp}/p_\perp = 0.01 \oplus 0.0026 p_\perp$, where $p_\perp$ is the track momentum transverse to the beam axis in GeV/c. Including the uncertainty on the primary interaction point (IP), the resolution on the charged-track impact parameter (d) projected in the plane perpendicular to the beamline is $\sigma_d = 11 \oplus 70/(p_\perp \sqrt{\sin\theta})$ μm, where θ is the polar angle with respect to the beamline. This results in a mean resolution on reconstructed 2-prong vertices (Section 3) of $\sigma_{V_{\parallel(\perp)}} = 400$ (25) μm for the projection on an axis along (perpendicular to) the vertex flight direction. The LAC electromagnetic energy scale was calibrated from the measured $\pi^0 \rightarrow \gamma\gamma$ signal [21, 22]; the electromagnetic energy resolution is $\sigma_E/E \approx 0.15/\sqrt{E(\mathrm{GeV})}$.

The trigger and initial selection of hadronic events are described in [23]. A set of cuts was applied to the data to select well-measured tracks and events well-contained within the detector acceptance. Charged tracks were required to have a distance of closest approach transverse to the beam axis within 5 cm, and within 10 cm along the axis from the measured interaction point, as well as $|\cos\theta| < 0.80$, and $p_\perp > 0.15$ GeV/c. Events were required to have a minimum of seven such tracks, a thrust axis [24] polar angle θ_T within $|\cos\theta_T| < 0.70$, and a charged visible energy E_{vis} of at least 20 GeV, which was calculated from the selected tracks assigned the charged pion mass. From our 1993-95 data sample 108650 events passed these cuts. The efficiency for selecting hadronic events satisfying the $|\cos\theta_T|$ cut was estimated to be above 96%. The background in the selected event sample was estimated to be $0.1 \pm 0.1\%$, dominated by $Z^0 \rightarrow \tau^+\tau^-$ events.

Calorimeter clusters used in the subsequent jet-finding analysis (Section 4) were required to comprise at least two calorimeter towers, each containing an energy of at least 100 MeV, and to have a total energy greater than 250 MeV. Electromagnetic clusters used in the non-B-associated neutral energy measurement were further required to have less than the smaller of, 25% of their energy and 600 MeV, in the hadronic section of the LAC.

The efficiency for reconstructing B hadrons, the background in the selected sample, and the resolution of the method were evaluated (Sections 3 and 4) using a detailed Monte Carlo (MC) simulation. The JETSET 7.4 [25] event generator was used, with parameter values tuned to hadronic e^+e^- annihilation data [26], combined with a simulation of B-decays tuned to $\Upsilon(4S)$ data [27] and a simulation of the SLD based on GEANT 3.21 [28]. Inclusive distributions of single particle and event topology observables in hadronic events were found to be well-described by the simulation [29]. There is now evidence that roughly 21% of all promptly-produced B hadrons in $Z^0 \rightarrow b\bar{b}$ events are B^{**} mesons [30]; since JETSET does not produce B^{**} mesons we have corrected the simulation to account for them. Using an event weighting technique we produced a generator-level distribution of B hadron energies in which the energy E_B of 20.7% of all B hadrons was adjusted to be $E_B - E_\pi$, where the pion energy E_π was produced according to an isotropic 2-body decay distribution for $\mathrm{B}^{**} \rightarrow \mathrm{B}\pi^{\pm}$, assuming a B^{**} mass of 5.7 GeV/c^2. Uncertainties in this simulation of B^{**} production were taken into account in the systematic errors (Section 7).

3 B Hadron Selection

Hadronic events were required to contain a lepton candidate within the barrel tracking system with $|\cos\theta| < 0.7$. We then applied the JADE jet-finding algorithm [31] to the LAC clusters in each selected event to define a jet topology. With a jet-resolution criterion of $y_c = 0.07$, 82.9% of the events were classified as 2-jet-like and 17.1% as 3-jet-like. Kinematic information based on this topological classification was used subsequently (Section 4) in the calculation of the B hadron energy. Events in which the lepton had a transverse momentum w.r.t. its jet axis, p_t, of at least 1 GeV/c were retained for further analysis. In jets containing more than one such lepton only the highest-p_t lepton was labelled for association with a D vertex and any lower-momentum leptons were used in the D-vertex-finding.

In each selected jet we then searched for a secondary D vertex among the non-lepton tracks. Tracks were required to comprise at least 40 CDC hits and one VXD hit, to be well contained within the CDC with $|\cos\theta| \leq 0.70$, to have momentum in the range $0.15 < p < 55$ GeV/c, and to have a transverse impact parameter, normalised by its error, of $d/\sigma_d > 1$. Tracks from K^0_s and Λ^0 decays and γ conversions were suppressed by requiring the distance of closest approach to the IP in the planes both perpendicular to, and containing, the beamline to be less than 1 cm. Two-prong vertices were first formed from all pairs of tracks whose distance-of-closest-approach was less than 0.012 cm and whose fit to a vertex satisfied $\chi^2 < 5$. A multi-prong D-vertex candidate was then defined to comprise the tracks in all accepted two-prong vertices in the jet, and to be located at the position of the two-prong vertex containing the track with the largest normalised transverse impact parameter d/σ_d.

The tracks in each D vertex were each assigned the charged pion mass and were then combined by adding their four-vectors to obtain the vertex invariant mass, m_D, and the vertex momentum vector. The vertex flight distance from the IP was projected onto the jet axis to obtain the quantity r_D. Events were retained if at least one jet contained a D vertex with $0.3 < m_D < 1.9$ GeV/c^2, $r_D > 0.05$ cm, r_D normalised by its error larger than unity, and the distance-of-closest-approach between the lepton track and the extrapolated D-vertex momentum vector was less than 0.012 cm. The lepton and D-vertex tracks were then fitted to a common candidate B vertex. The combined D-vertex and lepton invariant mass, m_B, and the projection of the vector between the B- and D-vertex positions onto the D-vertex momentum vector, r_B, were calculated. Events were selected in which $m_B < 4.5$ GeV/c^2, $r_B > 0.025$ cm, and r_B normalized by its error was larger than unity.

For the selected events, distributions of the number of tracks per D vertex, N_D, and of m_D, r_D, m_B, and r_B are shown in Fig. 1. Also shown are the simulated distributions in which the contribution from selected true $\mathrm{B} \rightarrow \mathrm{D}l\mathrm{X}$ decays is indicated. In Fig. 2 the distributions of lepton transverse momentum with respect to the jet axis, p_t, are shown for candidates passing all cuts except the requirement that p_t be above 1 GeV/c; the simulated distributions are also shown, and the contributions from different processes are indicated. The final sample comprises 597 events, 293 in the muon, and 304 in the electron, channels. Using the simulation we estimate that the purity of this sample, defined to be the fraction of the tagged events whose identified leptons l are from true $\mathrm{B} \rightarrow \mathrm{D}l\mathrm{X}$ decays, is 69.2%; a further 18% of the selected events contain B decays with a cascade, punch-through or mis-identified lepton, and are still useful. The estimated composition of the $\mathrm{b}\bar{\mathrm{b}}$ events in terms of the B hadron species is shown in Table 1. The remaining 12.8% of the event sample comprises non-$\mathrm{b}\bar{\mathrm{b}}$ events. The efficiency for selecting B hadron decays in the selected hadronic event sample is shown, as a function of x_{E_B}, in Fig. 3; the overall efficiency is 1.1%.

4 Measurement of the B Energies

In each selected event we first defined the jet energies by using kinematic information. The 2-jet events were divided into two hemispheres by the plane normal to the thrust axis and the jet in each hemisphere was assigned the beam energy. For the 3-jet events we corrected the jet energies according to the angles between the jet axes, assuming energy and momentum conservation and massless kinematics. Labelling the jets arbitrarily 1, 2 and 3, and the corresponding inter-jet angles θ_{23}, θ_{13} and θ_{12}, the corrected energy of jet 1 is given by:

$$E_1 = \sqrt{s}(\sin\theta_{23})/(\sin\theta_{12} + \sin\theta_{23} + \sin\theta_{13}), \tag{1}$$

with corresponding expressions for jets 2 and 3. This procedure results in improved jet energy resolution.

We then proceeded to reconstruct the B hadron energy E_B^{Rec}:

$$E_B^{Rec} \quad = \quad E_{jet} - E_{frag}, \tag{2}$$

where E_{jet} is the energy of the jet containing the candidate B vertex and E_{frag} is the energy in the same jet that is not attributed to the B,

$$E_{frag} \quad = \quad f^{chg}\, E_{frag}^{chg} + f^{neu}\, E_{frag}^{neu} \tag{3}$$

where E_{frag}^{chg} and E_{frag}^{neu} are the measured charged and neutral energy components respectively, and f^{chg} and f^{neu} are correction factors described below. We define E_{frag}^{chg} to be the sum of the energy, using the momentum and assuming the pion mass, of all the charged tracks in the jet excluding the candidate B-vertex tracks; E_{frag}^{neu} is defined to be the sum of the energy of the electromagnetic calorimeter clusters in the jet that are not associated with charged tracks. A cluster was defined as unassociated if it had no charged track extrapolating to it to within an angle $4\sigma_{cl}$ from its centroid, where $\sigma_{cl} = \sqrt{{\sigma_{cl}^{\theta}}^2 + {\sigma_{cl}^{\phi}}^2}$ and σ_{cl}^{θ} and σ_{cl}^{ϕ} are the measured cluster widths in polar- and azimuthal-angle, respectively. The distributions of E_{frag}^{chg} and E_{frag}^{neu} are shown in Fig. 4.

This procedure will *a priori* misassign the energy of any unassociated neutral particle from the D decay to the non-B energy E_{frag}. Similarly, the energy of any charged track from the D decay that is not associated with the reconstructed D vertex will be misassigned to E_{frag}. We have used our MC simulation to study these effects and show in Fig. 5 the correlation between the reconstructed and true values of E_{frag}^{neu} and E_{frag}^{chg}. As expected, both the charged and neutral components are typically slightly overestimated by the reconstruction method. We fitted an *ad hoc* second-order polynomial to each correlation to determine an average energy-dependent correction factor, f^{chg} (f^{neu}) (Eq. 3), which we applied to the non-B charged (neutral) energy component E_{frag}^{chg} (E_{frag}^{neu}) of each tagged jet in the data sample. Uncertainties in these corrections were included in the systematic errors (Section 7).

We have used our simulation to estimate the resolution of the method for reconstructing the B hadron energy. We compared the reconstructed scaled B energy $x_{E_B}^{rec}$ with the input scaled energy $x_{E_B}^{true}$ and show in Fig. 6 the distribution of the quantity $(x_{E_B}^{true} - x_{E_B}^{rec})/x_{E_B}^{true}$. The resolution may be characterised by a parametrisation comprising the sum of two Gaussian distributions. The result of such a fit, in which the Gaussian centers, normalisations and widths were allowed to vary, is shown in Fig. 6. The narrower Gaussian of width $\sigma = 0.10$ represents 65% of the fitted area, and the wider Gaussian of width $\sigma = 0.33$ represents the remainder. It can be seen from Fig. 6 that the population corresponding to the 'inner core' is somewhat underestimated by this technique since the parametrisation does not describe the central bin. We repeated this exercise in subset regions of $x_{E_B}^{true}$ and found the inner core resolution (population) to be 0.27 (84%) for $0.0 < x_{E_B}^{true} < 0.6$, 0.09 (70%) for $0.6 < x_{E_B}^{true} < 0.8$, and 0.06 (79%) for $0.9 < x_{E_B}^{true} < 1.0$; as expected the resolution is better for more energetic B hadrons. Choosing the bin width to be roughly half of our mean resolution we show the measured distribution of $x_{E_B}^{rec}$, $D^{data}(x_{E_B}^{rec})$, in Fig. 7. Also shown in this figure is the simulated distribution in which the background contribution from non-$b\bar{b}$ events is indicated.

5 Comparison with Model Predictions

It is interesting to compare our measured B hadron energy distribution with the theoretical predictions. The event generator used in our simulation is based on a perturbative QCD 'parton shower' for production of quarks and gluons, together with the phenomenological Peterson function [6] (Table 2) to account for the fragmentation of b and c quarks into B and D hadrons, respectively, within the iterative Lund string hadronisation mechanism [25]; this simulation yields a generator-level primary B-hadron energy distribution with $< x_{E_B} > = 0.693$*. It is apparent (Fig. 7) that this simulation does not reproduce the data well; the χ^2 for the comparison is 36.7 for 15 bins.

We have also considered alternative forms of the fragmentation function based on the phenomenological model of the Lund group [7], the perturbative QCD calculations of Braaten *et al.* [4], (BCFY) and of Nason *et al.* [2] (NCM), as well as *ad hoc* parametrisations based on a function used by the ALEPH Collaboration [12] and on a third-order polynomial. These functions are listed in Table 2.

In order to make a consistent comparison of each function with the data we adopted the following procedure. Starting values of the arbitrary parameters were assigned and the corresponding distribution of scaled primary B hadron energies, $D^{MC}(x_{E_B}^{true})$, was reproduced in our MC-generated $b\bar{b}$ event sample, *before* simulation of the detector, by weighting events accordingly. The resulting distribution, after simulation of the detector, application of the analysis cuts and background subtraction, of reconstructed B hadron energies, $D^{MC}(x_{E_B}^{rec})$, was then compared with the background-subtracted

*We used a value of the Peterson function parameter $\epsilon_b = 0.006$ [32].

data distribution and the χ^2 value was calculated. This process was iterated to find the minimum in χ^2, yielding a parameter set that gives an optimal description of the reconstructed data by the input fragmentation function. This procedure was applied for each function listed in Table 2. The fitted parameters and minimum χ^2 values are listed in Table 3, and the corresponding $D^{MC}(x_{E_B}^{rec})$ are compared with the data in Fig. 8. Each function reproduces the data. We conclude that, within our resolution and with our current data sample, we are unable to distinguish between these functions. It should be noted, however, that the optimal third-order polynomial function has a small negative minimum point in the region around $x_{E_B}^{true} = 0.2$; since this behaviour is unphysical we did not consider this function further in the analysis.

6 Correction of the B Energy Distribution

In order to compare our results with those from other experiments it is necessary to correct the reconstructed scaled B hadron energy distribution $D^{data}(x_{E_B}^{rec})$ for the effects of non-B backgrounds, detector acceptance, event selection and analysis bias, and initial-state radiation, as well as for bin-to-bin migration effects caused by the finite resolution of the detector and the analysis technique. We also corrected for the effects of B** decays (Section 2) to derive the primary B hadron energy distribution. We applied a 15×15 matrix unfolding procedure to $D^{data}(x_{E_B}^{rec})$ to obtain an estimate of the true distribution $D^{data}(x_{E_B}^{true})$:

$$D^{data}(x_{E_B}^{true}) \quad = \quad \epsilon^{-1}(x_{E_B}^{true}) \cdot E(x_{E_B}^{true}, x_{E_B}^{rec}) \cdot (D^{data}(x_{E_B}^{rec}) - S(x_{E_B}^{rec})) \tag{4}$$

where S is a vector representing the background contribution, E is a matrix to correct for bin-to-bin migrations, and ϵ is a vector representing the efficiency for selecting true B hadron decays for the analysis.

The matrices S, E and ϵ were calculated from our MC simulation; the elements of ϵ are shown in Fig. 3. The matrix E incorporates a convolution of the input fragmentation function with the resolution of the detector. We used in turn the Peterson, Lund, BCFY, NCM and ALEPH functions, with the optimised parameters listed in Table 3, to produce both a generator-level input primary B hadron energy distribution $D^{MC}(x_{E_B}^{true})$, and a reconstructed distribution $D^{MC}(x_{E_B}^{rec})$, as discussed in the previous section. In each case E was evaluated by examining the population migrations of true B hadrons between bins of the input scaled B energy, $x_{E_B}^{true}$, and the reconstructed scaled B energy, $x_{E_B}^{rec}$.

The data were then unfolded according to Eq. (4) to yield $D^{data}(x_{E_B}^{true})$, which is shown for each input fragmentation function in Fig. 9. It can be seen that the shapes of $D^{data}(x_{E_B}^{true})$ differ systematically among the assumed input fragmentation functions. These difference were used to assign systematic errors, as discussed in the next section.

7 Systematic Errors

We have considered sources of systematic uncertainty that potentially affect our measurement of the B-hadron energy distribution. These may be divided into uncertainties in modelling the detector and uncertainties on experimental measurements serving as input parameters to the underlying physics modelling. For these studies our standard simulation, employing the Peterson fragmentation function, was used.

The uncertainty on the correction of the non-B neutral jet energy component E_{frag}^{neu} (Section 4) was estimated by changing the LAC cluster-energy selection requirement from 100 to 200 MeV, and by varying the LAC electromagnetic energy scale within our estimated uncertainty of $\pm 2.2\%$ of its nominal value [21]. In each case the difference in results relative to our standard procedure was taken as the systematic uncertainty. A large source of detector modelling uncertainty was found to relate to knowledge of the charged tracking efficiency of the detector, which we varied by our estimated uncertainty of $\pm 2.4\%$. In addition, in each bin of $x_{E_B}^{rec}$, we varied the estimated contribution from fake leptons in the data sample (Fig. 2) by $\pm 25\%$. These uncertainties were assumed to be uncorrelated and were added in quadrature to obtain the detector modelling uncertainty in each bin of x_{E_B}.

As a cross-check we also varied the event selection requirements. The thrust-axis containment cut was varied in the range $0.65 < |\cos\theta_T| < 0.70$, the minimum number of charged tracks required was increased from 7 to 8, and the total charged-track energy requirement was increased from 20 to 22 GeV. In each case results consistent with the standard selection were obtained. As a further cross-check on jet axis modelling we systematically varied y_c in the range $0.01 \leq y_c \leq 0.15$ and repeated the analysis; results consistent with the standard analysis were obtained.

A large number of measured quantities relating to the production and decay of charm and bottom hadrons are used as input to our simulation. In $\mathrm{b\bar{b}}$ events we have considered the uncertainties on: the branching fraction for $Z^0 \rightarrow \mathrm{b\bar{b}}$; the rates of production of B_u, B_d and B_s mesons, and B baryons; the rate of production of B^{**} mesons, and the B^{**} mass; the branching ratios for $\mathrm{B} \rightarrow \mathrm{D}^*$ and $\mathrm{B} \rightarrow \mathrm{D}^{**}$; the lifetimes of B mesons and baryons; and the average charged multiplicity of B hadron decays. In $\mathrm{c\bar{c}}$ events we have considered the uncertainties on: the branching fraction for $Z^0 \rightarrow \mathrm{c\bar{c}}$; the charmed hadron fragmentation function; the rates of production of D^0, D^+ and D_s mesons, and charmed baryons; and the charged multiplicity of charmed hadron decays. We have also considered the rate of production of $\mathrm{s\bar{s}}$ in the jet fragmentation process, and the production of secondary $\mathrm{b\bar{b}}$ and $\mathrm{c\bar{c}}$ from gluon splitting. The world-average values [9, 32] of these quantities used in our simulation, as well as the respective uncertainties, are listed in Table 4.

The variation of each quantity within its uncertainty was produced in turn in our simulated event sample using an event weighting technique [32]. The matrices S and E (Section 6) were then reevaluated using the simulated events, and the data were recorrected. In each case the deviation w.r.t. the standard corrected result was taken as a separate systematic error. These uncertainties were conservatively assumed to be uncorrelated and were added in quadrature to obtain a total physics modelling uncertainty in each bin of x_{E_B}.

The model-dependence of the unfolding procedure was estimated by considering the envelope of the unfolded results illustrated in Fig. 9. In each bin of x_{E_B} we calculated the average value of the five unfolded results, as well as the r.m.s. deviation. The average value was taken as our central value in each bin, and the r.m.s. value was assigned as the respective unfolding uncertainty.

8 Summary and Conclusions

We have used the precise SLD tracking system to reconstruct the energies of B hadrons in $e^+e^- \rightarrow Z^0$ events via the B $\rightarrow$ DlX decay mode. We estimate our resolution on the B energy to be about 10% for roughly 65% of the reconstructed decays. The distribution of reconstructed scaled B hadron energy, $D(x_{E_B}^{rec})$, was compared with perturbative QCD and phenomenological model predictions; the calculations of Braaten, Cheung and Yuan and of Nason, Colangelo and Mele are consistent with our data, as are the phenomenological models of Peterson *et al.* and of the Lund group. The distribution was then corrected for bin-to-bin migrations caused by the resolution of the method and for selection efficiency, as well as for the effects of B** production, to derive the energy distribution of primary B hadrons produced by Z^0 decays. Systematic uncertainties in the correction were considered. The final corrected x_{E_B} distribution $D(x_{E_B})$ is listed in Table 5 and shown in Fig. 10; the statistical, experimental systematic, and unfolding uncertainties are indicated separately.

It is conventional to evaluate the mean of this distribution, $< x_{E_B} >$. For each of the five functions used to correct the data we evaluated $< x_{E_B} >$ from the distribution that corresponds to the optimised parameters; these are listed in Table 3. We took the average of the five values of $< x_{E_B} >$ as our central result, and defined the unfolding uncertainty to be the r.m.s. deviation. We list in Table 4 the errors on $< x_{E_B} >$ resulting from the study of detector and physics modelling described in Section 7. We obtained:

$$< x_{E_B} > \quad = \quad 0.716 \ \pm \ 0.011(\text{stat.}) \ ^{+0.009}_{-0.011} \ (\text{exp. syst.}) \ \pm \ 0.019 \ (\text{unfolding}),$$

where the systematic error is the sum in quadrature of the individual contributions listed in Table 4. It can be seen that $< x_{E_B} >$ is relatively insensitive to the variety of allowed forms of the shape of the fragmentation function $D(x_{E_B})$.

Our results are in agreement with a previous measurement of the shape of the primary B hadron energy distribution at the Z^0 resonance [12], as well as with measurements of the shape [13] and mean value [10] of the distribution for weakly-decaying B hadrons, after taking account of our estimate that the latter $< x_{E_B} >$ value is about 0.015 lower. Combining all systematic errors in quadrature we obtain $< x_{E_B} > = 0.716 \ \pm \ 0.011$ (stat.) $^{+0.021}_{-0.022}$ (syst.).

Acknowledgements

We thank the personnel of the SLAC accelerator department and the technical staffs of our collaborating institutions for their outstanding efforts on our behalf.

*This work was supported by Department of Energy contracts: DE-FG02-91ER40676 (BU), DE-FG03-91ER40618 (UCSB), DE-FG03-92ER40689 (UCSC), DE-FG03-93ER40788 (CSU), DE-FG02-91ER40672 (Colorado), DE-FG02-91ER40677 (Illinois), DE-AC03-76SF00098 (LBL), DE-FG02-92ER40715 (Massachusetts), DE-FC02-94ER40818 (MIT), DE-FG03-96ER40969 (Oregon), DE-AC03-76SF00515 (SLAC), DE-FG05-91ER40627 (Tennessee), DE-FG02-95ER40896 (Wisconsin), DE-FG02-92ER40704 (Yale); National Science Foundation grants: PHY-91-13428 (UCSC), PHY-89-21320 (Columbia), PHY-92-04239 (Cincinnati), PHY-95-10439 (Rutgers), PHY-88-19316 (Vanderbilt), PHY-92-03212 (Washington); The UK Particle Physics and Astronomy Research Council (Brunel and RAL); The Istituto Nazionale di Fisica Nucleare of Italy (Bologna, Ferrara, Frascati, Pisa, Padova, Perugia); The Japan-US Cooperative Research Project on High Energy Physics (Nagoya, Tohoku); The Korea Science and Engineering Foundation (Soongsil).

References

[1] See *eg.* J.D. Bjorken, Phys. Rev. **D17** (1978) 171.

[2] B. Mele and P. Nason, Phys. Lett. **B245** (1990) 635.
B. Mele and P. Nason, Nucl. Phys. **B361** (1991) 626.
G. Colangelo and P. Nason, Phys. Lett. **B285** (1992) 167.

[3] Yu. L. Dokshitzer, V.A. Khoze, S.I. Troyan, Phys. Rev. **D53** (1996) 89.

[4] E. Braaten, K. Cheung, T.C. Yuan, Phys. Rev. **D48** (1993) R5049.
E. Braaten, K. Cheung, S. Fleming, T.C. Yuan, Phys. Rev. **D51** (1995) 4819.

[5] M.G. Bowler, Z. Phys. **C11** (1981) 169.

[6] C. Peterson, D. Schlatter, I. Schmitt and P.M. Zerwas, Phys. Rev. **D27** (1983) 105.

[7] B. Andersson, G. Gustafson, G. Ingelman, T. Sjöstrand, Phys. Rep. **97** (1983) 32.

[8] L. Randall, N. Rius, Nucl. Phys. **B441** (1995) 167.

[9] The LEP Electroweak Working Group, D. Abbaneo *et al.*, LEPHF/96-01 (July 1996).

[10] ALEPH Collab., D. Buskulic *et al.*, Z. Phys. **C62** (1994) 179.
DELPHI Collab., P. Abreu *et al.*, Z. Phys. **C66** (1995) 323.
L3 Collab., O. Adeva *et al.*, Phys Lett. **B261** (1991) 177.
OPAL Collab., P.D. Acton *et al.*, Z. Phys. **C60** (1993) 199.

[11] See *eg.* D.H. Saxon in 'High Energy Electron-Positron Physics', Eds. A. Ali, P. Söding, World Scientific 1988, p. 539.

[12] ALEPH Collab., D. Buskulic *et al.*, Phys. Lett. **B357** (1995) 699.

[13] OPAL Collab., G. Alexander *et al.*, Phys. Lett. **B364** (1995) 93.

[14] ALEPH Collab., D. Buskulic *et al.*, Phys. Lett. **B356** (1995) 409.
OPAL Collab., G. Alexander *et al.*, Z. Phys. **C70** (1996) 357.
DELPHI Collab., P. Abreu *et al.*, Phys. Lett. **B301** (1993) 145.
L3 Collab., M. Acciarri *et al.*, Phys. Lett. **B335** (1994) 542.
SLD Collab., K. Abe *et al.*, Nucl. Phys. B (Proc. Suppl.) **50** (1996) 71.

[15] SLD Design Report, SLAC Report 273 (1984).

[16] M.D. Hildreth *et al.*, IEEE Trans. Nucl. Sci. **42** (1994) 451.

[17] C. J. S. Damerell *et al.*, Nucl. Inst. Meth. **A288** (1990) 236.

[18] D. Axen *et al.*, Nucl. Inst. Meth. **A328** (1993) 472.

[19] A. C. Benvenuti *et al.*, Nucl. Inst. Meth. **A290** (1990) 353.

[20] SLD Collab., K. Abe *et al.*, Phys. Rev. Lett. **74** (1995) 2895.

[21] S. Gonzalez–Martirena, MIT Ph.D. Thesis, SLAC–Report–439 (1994).

[22] E. Church, Univ. of Washington Ph.D. Thesis, SLAC–Report–495 (1996).

[23] SLD Collab., K. Abe *et al.*, Phys. Rev. Lett. **73** (1994) 25.

[24] S. Brandt *et al.*, Phys. Lett. **12** (1964) 57.
E. Farhi, Phys. Rev. Lett. **39** (1977) 1587.

[25] T. Sjöstrand, CERN-TH.7112/93 (1993).

[26] P. N. Burrows, Z. Phys. **C41** (1988) 375.
OPAL Collab., M.Z. Akrawy *et al.*, Z. Phys. **C47** (1990) 505.

[27] SLD Collab., K. Abe *et al.*, SLAC-PUB-7117; to appear in Phys. Rev. Lett.

[28] R. Brun *et al.*, Report No. CERN-DD/EE/84-1 (1989).

[29] SLD Collaboration, K. Abe *et al.*, Phys. Rev. **D51** (1995) 962.

[30] OPAL Collab., P.D. Acton *et al.*, Z. Phys. **C66** (1995) 19.
DELPHI Collab., P. Abreu *et al.*, Phys. Lett. **B345** (1995) 598.
ALEPH Collab., D. Buskulic *et al.*, Z. Phys. **C69** (1996) 393.

[31] JADE Collab., W. Bartel *et al.*, Z. Phys. **C33** (1986) 23.

[32] SLD Collab., K. Abe *et al.*, Phys. Rev. **D53** (1996) 1023.

[33] D. Coffman *et al.*, Phys. Lett. **B263** (1991) 135.

**List of Authors

K. Abe,(19) K. Abe,(30) T. Akagi,(28) N.J. Allen,(4) W.W. Ash,(28)† D. Aston,(28)
K.G. Baird,(24) C. Baltay,(34) H.R. Band,(33) M.B. Barakat,(34) G. Baranko,(9)
O. Bardon,(15) T. L. Barklow,(28) G.L. Bashindzhagyan,(18) A.O. Bazarko,(10)
R. Ben-David,(34) A.C. Benvenuti,(2) G.M. Bilei,(22) D. Bisello,(21) G. Blaylock,(16)
J.R. Bogart,(28) B. Bolen,(17) T. Bolton,(10) G.R. Bower,(28) J.E. Brau,(20)
M. Breidenbach,(28) W.M. Bugg,(29) D. Burke,(28) T.H. Burnett,(32) P.N. Burrows,(15)
W. Busza,(15) A. Calcaterra,(12) D.O. Caldwell,(5) D. Calloway,(28) B. Camanzi,(11)
M. Carpinelli,(23) R. Cassell,(28) R. Castaldi,(23)(a) A. Castro,(21) M. Cavalli-Sforza,(6)
A. Chou,(28) E. Church,(32) H.O. Cohn,(29) J.A. Coller,(3) V. Cook,(32) R. Cotton,(4)
R.F. Cowan,(15) D.G. Coyne,(6) G. Crawford,(28) A. D'Oliveira,(7) C.J.S. Damerell,(25)
M. Daoudi,(28) R. De Sangro,(12) R. Dell'Orso,(23) P.J. Dervan,(4) M. Dima,(8)
D.N. Dong,(15) P.Y.C. Du,(29) R. Dubois,(28) B.I. Eisenstein,(13) R. Elia,(28)
E. Etzion,(33) S. Fahey,(9) D. Falciai,(22) C. Fan,(9) J.P. Fernandez,(6) M.J. Fero,(15)
R. Frey,(20) T. Gillman,(25) G. Gladding,(13) S. Gonzalez,(15) E.L. Hart,(29)
J.L. Harton,(8) A. Hasan,(4) Y. Hasegawa,(30) K. Hasuko,(30) S. J. Hedges,(3)
S.S. Hertzbach,(16) M.D. Hildreth,(28) J. Huber,(20) M.E. Huffer,(28) E.W. Hughes,(28)

H. Hwang,[20] Y. Iwasaki,[30] D.J. Jackson,[25] P. Jacques,[24] J. A. Jaros,[28]
Z. Y. Jiang,[28] A.S. Johnson,[3] J.R. Johnson,[33] R.A. Johnson,[7] T. Junk,[28]
R. Kajikawa,[19] M. Kalelkar,[24] H. J. Kang,[26] I. Karliner,[13] H. Kawahara,[28]
H.W. Kendall,[15] Y. D. Kim,[26] M.E. King,[28] R. King,[28] R.R. Kofler,[16]
N.M. Krishna,[9] R.S. Kroeger,[17] J.F. Labs,[28] M. Langston,[20] A. Lath,[15]
J.A. Lauber,[9] D.W.G.S. Leith,[28] V. Lia,[15] M.X. Liu,[34] X. Liu,[6] M. Loreti,[21]
A. Lu,[5] H.L. Lynch,[28] J. Ma,[32] G. Mancinelli,[24] S. Manly,[34] G. Mantovani,[22]
T.W. Markiewicz,[28] T. Maruyama,[28] H. Masuda,[28] E. Mazzucato,[11]
A.K. McKemey,[4] B.T. Meadows,[7] R. Messner,[28] P.M. Mockett,[32]
K.C. Moffeit,[28] T.B. Moore,[34] D. Muller,[28] T. Nagamine,[28] S. Narita,[30]
U. Nauenberg,[9] H. Neal,[28] M. Nussbaum,[7]† Y. Ohnishi,[19] N. Oishi,[19]
D. Onoprienko,[29] L.S. Osborne,[15] R.S. Panvini,[31] C.H. Park,[27] H. Park,[20]
T.J. Pavel,[28] I. Peruzzi,[12][b] M. Piccolo,[12] L. Piemontese,[11] E. Pieroni,[23]
K.T. Pitts,[20] R.J. Plano,[24] R. Prepost,[33] C.Y. Prescott,[28] G.D. Punkar,[28]
J. Quigley,[15] B.N. Ratcliff,[28] T.W. Reeves,[31] J. Reidy,[17] P.L. Reinertsen,[6]
P.E. Rensing,[28] L.S. Rochester,[28] P.C. Rowson,[10] J.J. Russell,[28] O.H. Saxton,[28]
T. Schalk,[6] R.H. Schindler,[28] B.A. Schumm,[6] J. Schwiening,[28] S. Sen,[34]
V.V. Serbo,[33] M.H. Shaevitz,[10] J.T. Shank,[3] G. Shapiro,[14] D.J. Sherden,[28]
K.D. Shmakov,[29] C. Simopoulos,[28] N.B. Sinev,[20] S.R. Smith,[28] M.B. Smy,[8]
J.A. Snyder,[34] H. Staengle,[8] P. Stamer,[24] H. Steiner,[14] R. Steiner,[1]
M.G. Strauss,[16] D. Su,[28] F. Suekane,[30] A. Sugiyama,[19] S. Suzuki,[19]
M. Swartz,[28] A. Szumilo,[32] T. Takahashi,[28] F.E. Taylor,[15] E. Torrence,[15]
A.I. Trandafir,[16] J.D. Turk,[34] T. Usher,[28] J. Va'vra,[28] C. Vannini,[23] E. Vella,[28]
J.P. Venuti,[31] R. Verdier,[15] P.G. Verdini,[23] D.L. Wagner,[9] S.R. Wagner,[28]
A.P. Waite,[28] S.J. Watts,[4] A.W. Weidemann,[29] E.R. Weiss,[32] J.S. Whitaker,[3]
S.L. White,[29] F.J. Wickens,[25] D.C. Williams,[15] S.H. Williams,[28] S. Willocq,[28]
R.J. Wilson,[8] W.J. Wisniewski,[28] M. Woods,[28] G.B. Word,[24] J. Wyss,[21]
R.K. Yamamoto,[15] J.M. Yamartino,[15] X. Yang,[20] J. Yashima,[30] S.J. Yellin,[5]

C.C. Young,[28] H. Yuta,[30] G. Zapalac,[33] R.W. Zdarko,[28] and J. Zhou,[20]

[1]*Adelphi University, Garden City, New York 11530*

[2]*INFN Sezione di Bologna, I-40126 Bologna, Italy*

[3]*Boston University, Boston, Massachusetts 02215*

[4]*Brunel University, Uxbridge, Middlesex UB8 3PH, United Kingdom*

[5]*University of California at Santa Barbara, Santa Barbara, California 93106*

[6]*University of California at Santa Cruz, Santa Cruz, California 95064*

[7]*University of Cincinnati, Cincinnati, Ohio 45221*

[8]*Colorado State University, Fort Collins, Colorado 80523*

[9]*University of Colorado, Boulder, Colorado 80309*

[10]*Columbia University, New York, New York 10027*

[11]*INFN Sezione di Ferrara and Università di Ferrara, I-44100 Ferrara, Italy*

[12]*INFN Lab. Nazionali di Frascati, I-00044 Frascati, Italy*

[13]*University of Illinois, Urbana, Illinois 61801*

[14]*E.O. Lawrence Berkeley Laboratory, University of California, Berkeley, California 94720*

[15]*Massachusetts Institute of Technology, Cambridge, Massachusetts 02139*

[16]*University of Massachusetts, Amherst, Massachusetts 01003*

[17]*University of Mississippi, University, Mississippi 38677*

[18]*Moscow State University, Institute of Nuclear Physics 119899 Moscow, Russia*

[19]*Nagoya University, Chikusa-ku, Nagoya 464 Japan*

[20]*University of Oregon, Eugene, Oregon 97403*

[21]*INFN Sezione di Padova and Università di Padova, I-35100 Padova, Italy*

[22]*INFN Sezione di Perugia and Università di Perugia, I-06100 Perugia, Italy*

[23]*INFN Sezione di Pisa and Università di Pisa, I-56100 Pisa, Italy*

[24]*Rutgers University, Piscataway, New Jersey 08855*

[25] *Rutherford Appleton Laboratory, Chilton, Didcot, Oxon OX11 0QX United Kingdom*

[26] *Sogang University, Seoul, Korea*

[27] *Soongsil University, Seoul, Korea 156-743*

[28] *Stanford Linear Accelerator Center, Stanford University, Stanford, California 94309*

[29] *University of Tennessee, Knoxville, Tennessee 37996*

[30] *Tohoku University, Sendai 980 Japan*

[31] *Vanderbilt University, Nashville, Tennessee 37235*

[32] *University of Washington, Seattle, Washington 98195*

[33] *University of Wisconsin, Madison, Wisconsin 53706*

[34] *Yale University, New Haven, Connecticut 06511*

† *Deceased*

[a] *Also at the Università di Genova*

[b] *Also at the Università di Perugia*

B species	C (%)	ϵ (%)
B_u	43	92
B_d	43	87
B_s	10	89
B baryons	4	87

Table 1: The composition C of true $B \to Dl X$ decays in the final sample; ϵ is the fraction of each species whose D vertices are correctly reconstructed. In all cases the MC statistical errors are less than 2%.

Function Name	Functional form $D(x)$	Reference
Peterson	$\frac{1}{x}(1-\frac{1}{x}-\frac{\epsilon_b}{1-x})^{-2}$	[6]
Lund	$\frac{1}{x}(1-x)^a \exp(-bm_T^2/x)$	[7]
BCFY	$\frac{x(1-x^2)}{(1-(1-r)x)^6}[3-xf_1(r)+x^2f_2(r)-x^3f_3(r)+x^4f_4(r)]$	[4]
NCM	$\int dy\, g(x,y)y^\alpha(1-y)^\beta$	[2]
ALEPH	$\frac{1+b(1-x)}{x}(1-\frac{c}{x}-\frac{d}{1-x})^{-2}$	[12]
3^{rd}-order Polynomial	$1+bx+cx^2+dx^3$	

Table 2: Fragmentation functions used in comparison with the data. For the BCFY function $f_1(r)=3(3-4r)$, $f_2(r)=12-23r+26r^2$, $f_3(r)=(1-r)(9-11r+12r^2)$, and $f_4(r)=3(1-r)^2(1-r+r^2)$.

Function	χ^2/d.o.f.	parameters	$< x_{E_B} >$
Peterson	14.0/11	$\epsilon_b = 0.034 \pm 0.006^*$	0.717
Lund	9.6/10	$a = 1.7 \pm 0.2$ $b = 0.19 \pm 0.01$	0.743
BCFY	22.4/11	$r = 0.20 \pm 0.02$	0.705
NCM	15.9/11	$\alpha = 9 \pm 2$ $\beta = 44 \pm 8$	0.687
ALEPH	9.7/9	$b = 0.0 \pm 1.0$ $c = 0.78 \pm 0.05$ $d = 0.042 \pm 0.004$	0.730
3^{rd}-order polynomial	14.9/9	$b = -7.53 \pm 0.04$ $c = 16.49 \pm 0.07$ $d = -9.98 \pm 0.07$	–

Table 3: Results of optimisation of fragmentation functions to the reconstructed B hadron energy distribution. For the NCM fit the QCD parameters were fixed at Λ_f = 200 MeV and $\mu = m_b = 4.5$ GeV. * This value of ϵ_b refers to the B-hadron energy distribution; it should not be confused with the value of ϵ_b used as input in the JETSET model at the b-quark fragmentation level (Section 5), which is significantly lower.

Error source	Variation	Error (%)
DETECTOR MODELLING		
Neutral fragmentation energy:		
cluster energy scale	$\pm 2.2\%$	$^{+0.12}_{-0.27}$
min. clus energy	100^{-0}_{+100} MeV	$^{+0.00}_{-0.21}$
Tracking inefficiency	$2.4 \mp 2.4\%$	$^{+0.2}_{-1.0}$
Lepton mis-ID background	$\pm 25\%$	$^{+0.66}_{-0.65}$
PHYSICS MODELLING		
B meson / baryon lifetime	1.55 ± 0.05 / 1.10 ± 0.08 ps	$^{+0.11}_{-0.12}$
B^{**} production	$20.7 \pm 7\%$	$^{+0.68}_{-0.10}$
B^{**} mass	5.704 ± 0.020 GeV	$^{+0.03}_{-0.00}$
$f^* \equiv \Gamma(\mathrm{B}\rightarrow\mathrm{D}^*)/\Gamma(\mathrm{B}\rightarrow\mathrm{D})$	$f^{*}{}^{+0}_{-f^*/3}$	$^{+0.32}_{-0.00}$
$f^{**} \equiv \Gamma(\mathrm{B}\rightarrow\mathrm{D}^{**})/\Gamma(\mathrm{B}\rightarrow\mathrm{D})$	$f^{**} \pm f^{**}/3$	$^{+0.32}_{-0.21}$
B_u, B_d / B_s / b-baryon production	$40.1 \pm 20.0\%$ / $11.6 \pm 8.0\%$ / $7.0 \pm 4.0\%$	$^{+0.51}_{-0.48}$
B_u, B_d, B_s, b-baryon decay modes	$\pm 1\sigma$	$^{+0.11}_{-0.12}$
B-decay charged multiplicity	5.3 ± 0.2 tracks	$^{+0.25}_{-0.16}$
c-fragmentation: $< x_{E_D} >$	0.484 ± 0.008	± 0.01
D^0 / D^+ / D_s / c-baryon production	$56.0 \pm 5.3\%$ / $23.0 \pm 3.7\%$ / $12.0 \pm 7.0\%$ / $8.9 \pm 0.5\%$	± 0.01
D decay multiplicity	Ref. [33]	$^{+0.04}_{-0.05}$
$\mathrm{s\bar{s}}$ production	$\pm 10\%$	$^{+0.37}_{-0.40}$
R_b	0.2216 ± 0.0010	$^{+0.00}_{-0.01}$
R_c	0.16 ± 0.01	$^{+0.02}_{-0.04}$
$\mathrm{g} \rightarrow \mathrm{b\bar{b}}$ splitting	$\pm 50\%$	$^{+0.23}_{-0.30}$
$\mathrm{g} \rightarrow \mathrm{c\bar{c}}$ splitting	$\pm 50\%$	$^{+0.22}_{-0.25}$
Total		$^{+1.32}_{-1.48}$

Table 4: Systematic errors on $\langle x_{E_B} \rangle$.

x_{E_B} bin center	$1/\sigma d\sigma/dx_{E_B}$	Stat. error	Syst. error	Unfolding uncertainty
0.037	0.0	0.0	0.0	0.0
0.110	0.104	0.041	0.055	0.041
0.183	0.105	0.050	0.068	0.035
0.256	0.158	0.076	0.095	0.043
0.329	0.248	0.099	0.102	0.064
0.402	0.358	0.115	0.096	0.074
0.475	0.560	0.136	0.095	0.061
0.548	0.951	0.167	0.126	0.033
0.621	1.489	0.204	0.137	0.088
0.694	2.136	0.242	0.164	0.171
0.767	3.011	0.278	0.164	0.191
0.840	2.944	0.285	0.251	0.112
0.913	1.460	0.211	0.319	0.144
0.986	0.164	0.067	0.118	0.041

Table 5: The fully-corrected scaled B hadron energy distribution.

Figure Captions

Figure 1: Candidate D-vertex distributions: (a) number of tracks per vertex; (b) vertex mass; (c) projection of the vertex flight distance from the IP along the jet axis. Candidate B-vertex distributions: (d) vertex mass; (e) projection along the D-vertex momentum vector of the vector between the D vertex and the B vertex. Data (points with error bars) and simulation (solid histogram); the dashed histogram shows the simulated contribution from true B $\rightarrow$ DlX decays. In (a) all cuts were applied. In (b)-(e) all cuts were applied except those on the quantity shown, and these latter cut positions (see text) are indicated by arrows.

Figure 2: Distribution of (a) electron and (b) muon transverse momentum w.r.t. the jet axis in jets containing a selected D vertex and respective lepton. Data (points with error bars) and simulation (histogram). The composition of the simulated distributions in terms of leptons from B $\rightarrow$ l decays, cascade B $\rightarrow$ C $\rightarrow$ l decays, wrongly-assigned leptons, promptly produced C $\rightarrow$ l decays, and fake leptons is indicated.

Figure 3: The efficiency ϵ for selecting B hadron decays, as a function of scaled energy x_{E_B}. Note that the first bin (no point shown) is beneath the kinematic limit for x_{E_B}.

Figure 4: Distribution of non-B-associated (a) charged and (b) neutral energy in jets containing a candidate B $\rightarrow$ DlX decay. Data (points with error bars) and simulation (histogram).

Figure 5: Simulated correlation between the true and reconstructed values of the non-B-associated (a) neutral and (b) charged energy in jets containing a candidate B $\rightarrow$ DlX decay. In each bin of reconstructed energy the error bar represents the corresponding r.m.s. deviation in the true energy. Each line represents a fit to the correlation (see text).

Figure 6: Distribution of the normalised difference between the true and reconstructed B hadron energies in simulated events. The solid line is a fit of the sum of two Gaussian distributions (see text). The two component Gaussian distributions are indicated by the dashed lines.

Figure 7: The distribution of reconstructed scaled energies for B hadron candidates; data (points with error bars) and simulation (solid histogram). Also shown (dashed histogram) is the simulated contribution from non-$b\bar{b}$ events.

Figure 8: The background-subtracted distribution of reconstructed scaled B hadron energy. The data (points with error bars) are compared with simulations based on six different input B fragmentation functions (see text) represented by lines joining entries at the bin centers.

Figure 9: Data distribution of scaled B hadron energy corrected using simulations based on different input B fragmentation functions (see text): (a) ALEPH, (b) Peterson, (c) Lund, (d) BCFY and (e) NCM functions. Statistical error bars are shown; these are highly correlated between bins and among the five sets of results. (f) The five optimised functional forms used in the correction.

Figure 10: The final corrected distribution of scaled B hadron energies. In each bin the statistical error is indicated by the innermost error bar, the quadrature sum of statistical and experimental systematic errors by the middle error bar, and the quadrature sum of statistical, experimental systematic and unfolding errors by the outermost error bar. Note that the first bin (no point shown) is beneath the kinematic limit for x_{E_B}.

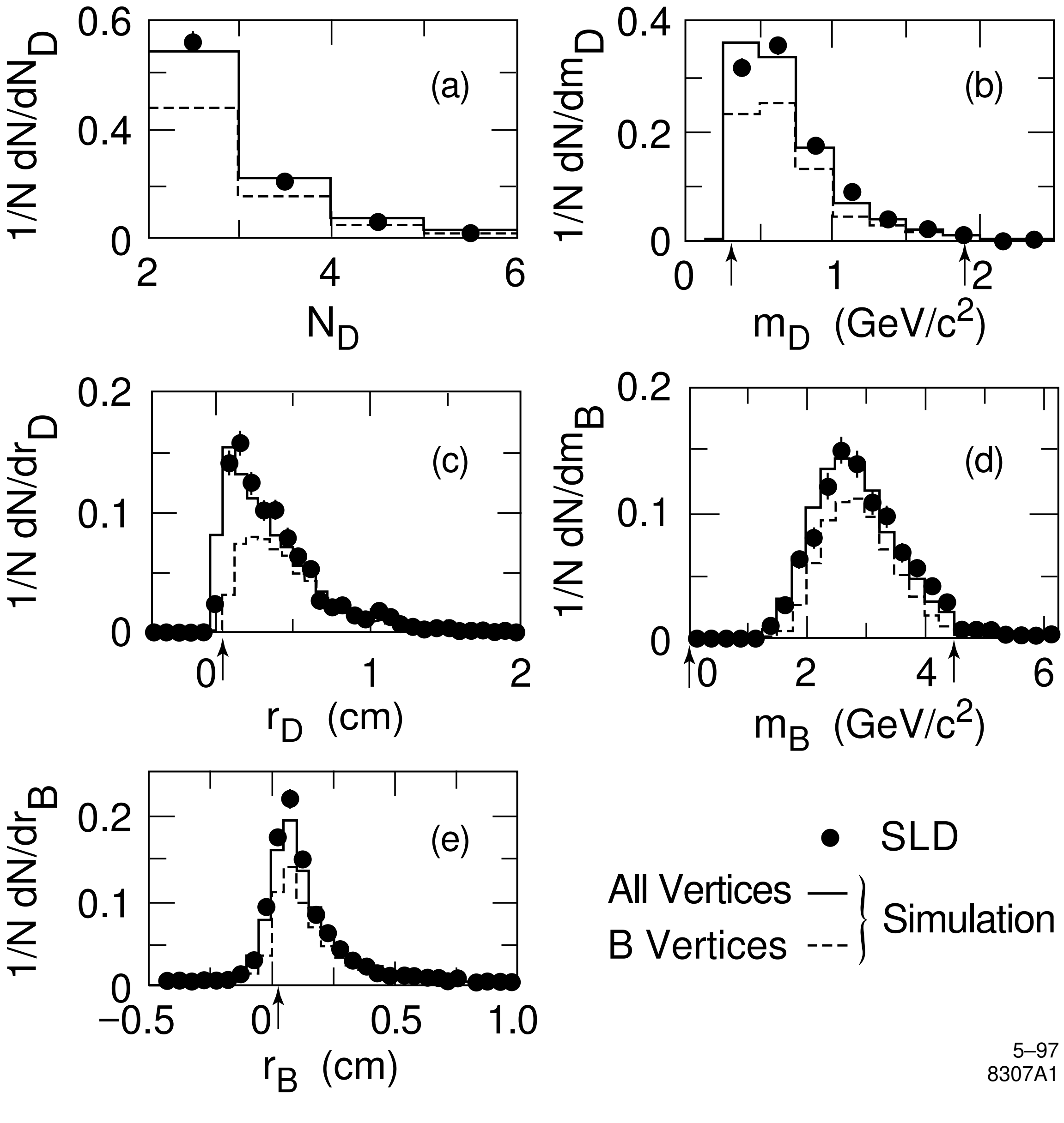

1/N dN/dN_D
N_D
(a)
1/N dN/dm_D
m_D (GeV/c^2)
(b)
1/N dN/dr_D
r_D (cm)
(c)
1/N dN/dm_B
m_B (GeV/c^2)
(d)
1/N dN/dr_B
r_B (cm)
(e)
SLD
All Vertices
B Vertices
Simulation
5–97
8307A1

Figure 1:

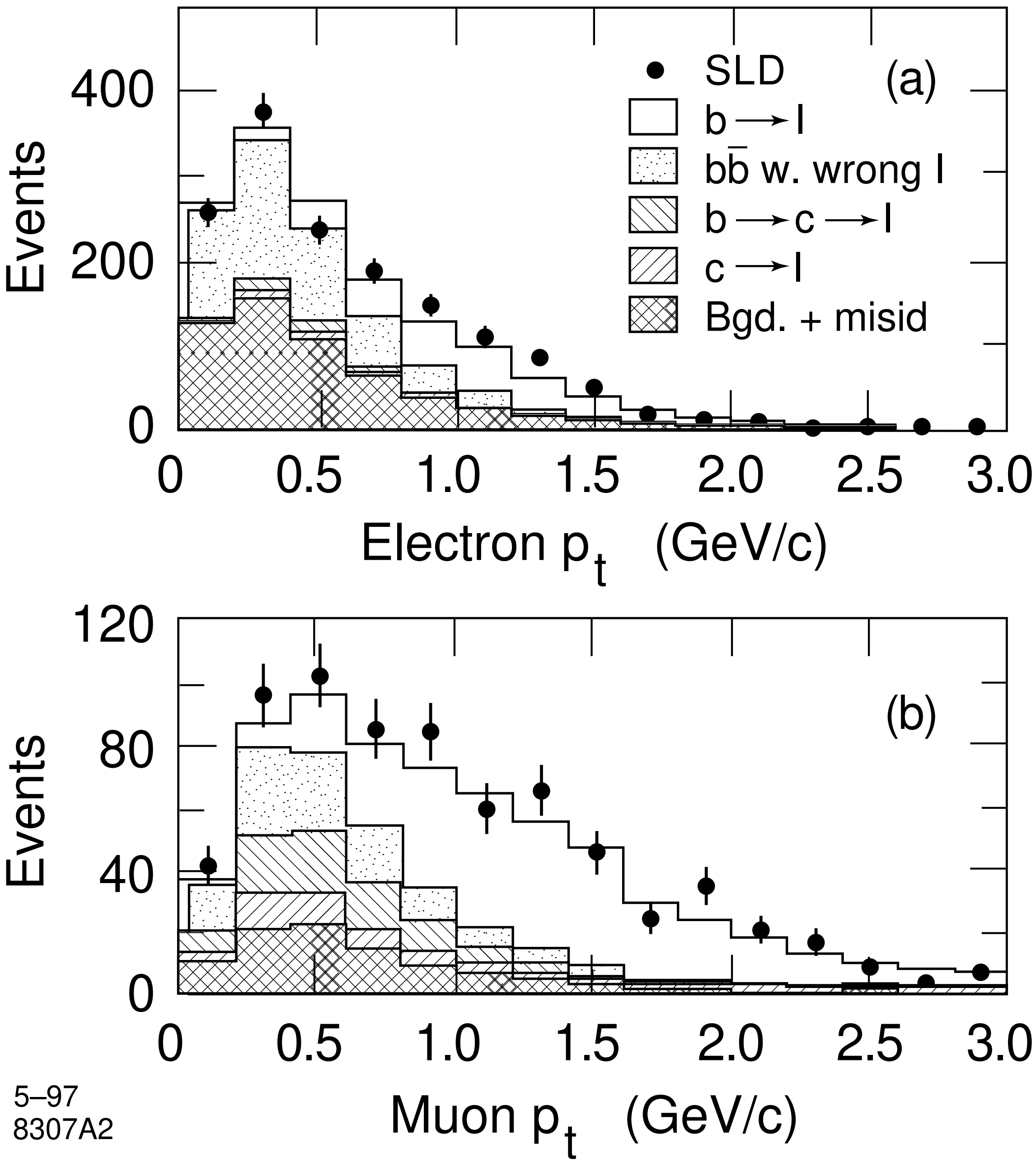
SLD
(a)
b → l
b$\bar{b}$ w. wrong l
b → c → l
c → l
Bgd. + misid
Events
0
200
400
0
0.5
1.0
1.5
2.0
2.5
3.0
Electron p_t (GeV/c)
Events
0
40
80
120
(b)
Muon p_t (GeV/c)
5–97
8307A2

Figure 2:

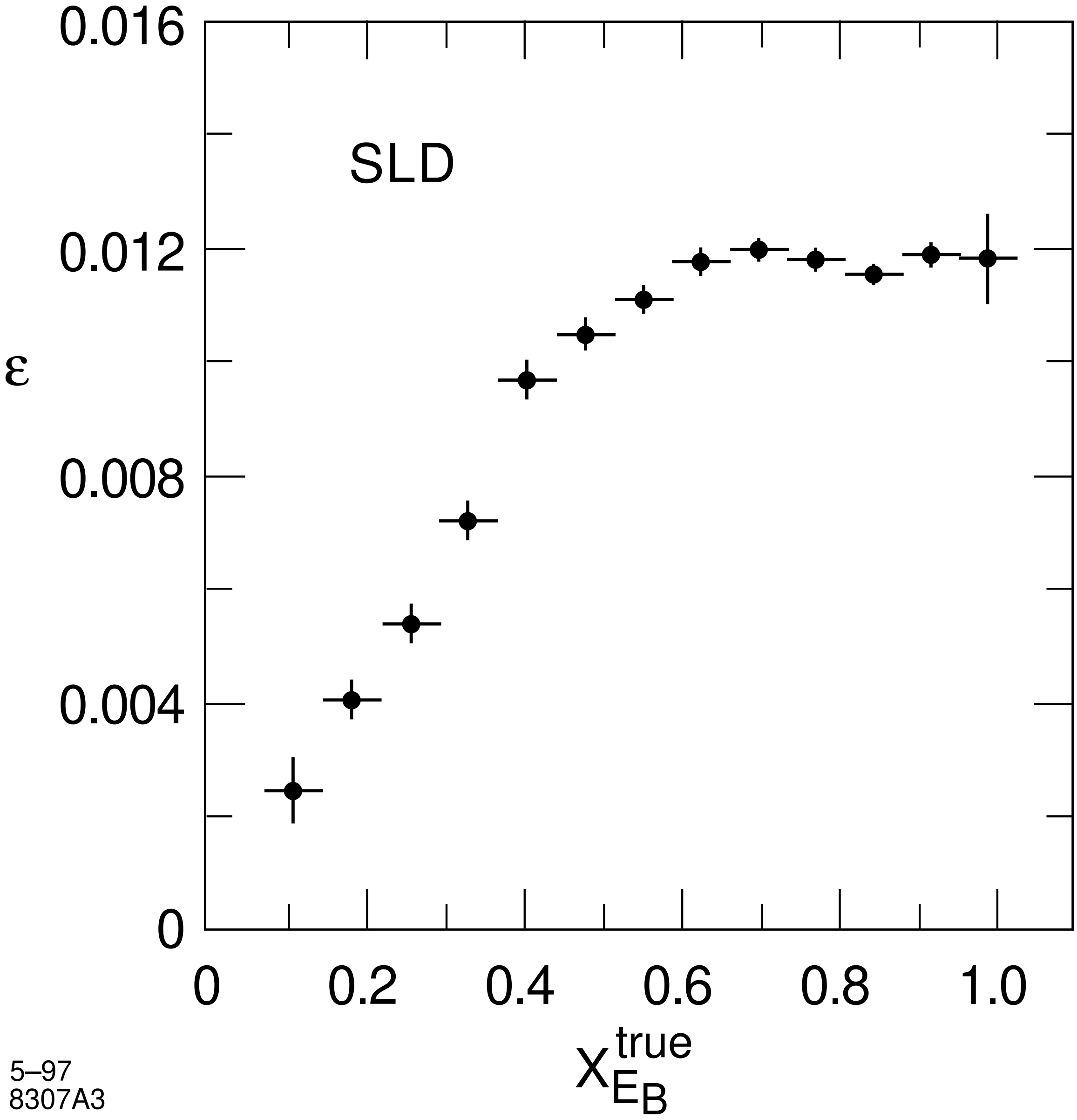

Figure 3:

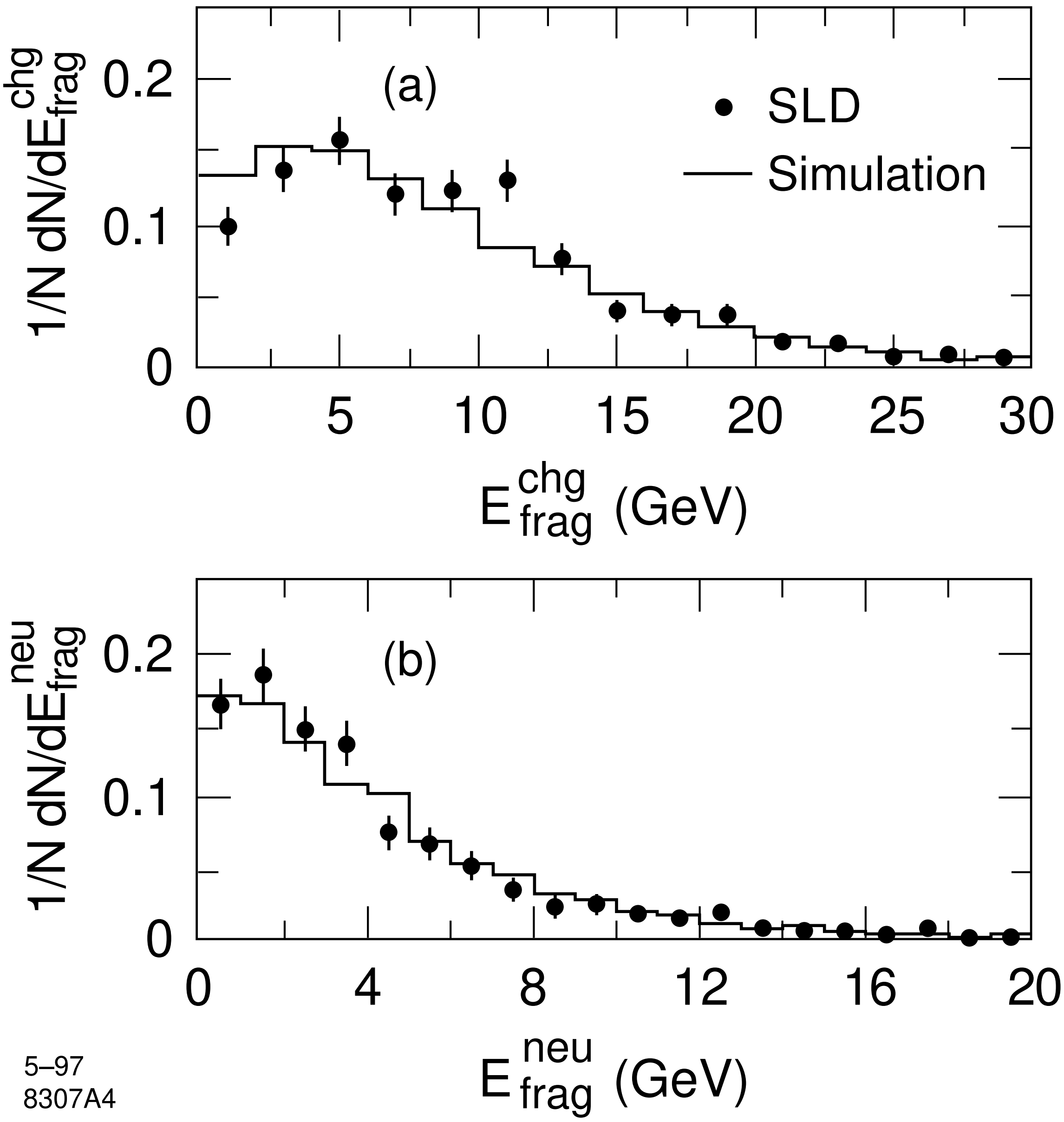

(a)
SLD
Simulation
1/N dN/dE$^{chg}_{frag}$
0
0.1
0.2
0
5
10
15
20
25
30
E$^{chg}_{frag}$ (GeV)
(b)
1/N dN/dE$^{neu}_{frag}$
0
0.1
0.2
0
4
8
12
16
20
E$^{neu}_{frag}$ (GeV)
5–97
8307A4

Figure 4:

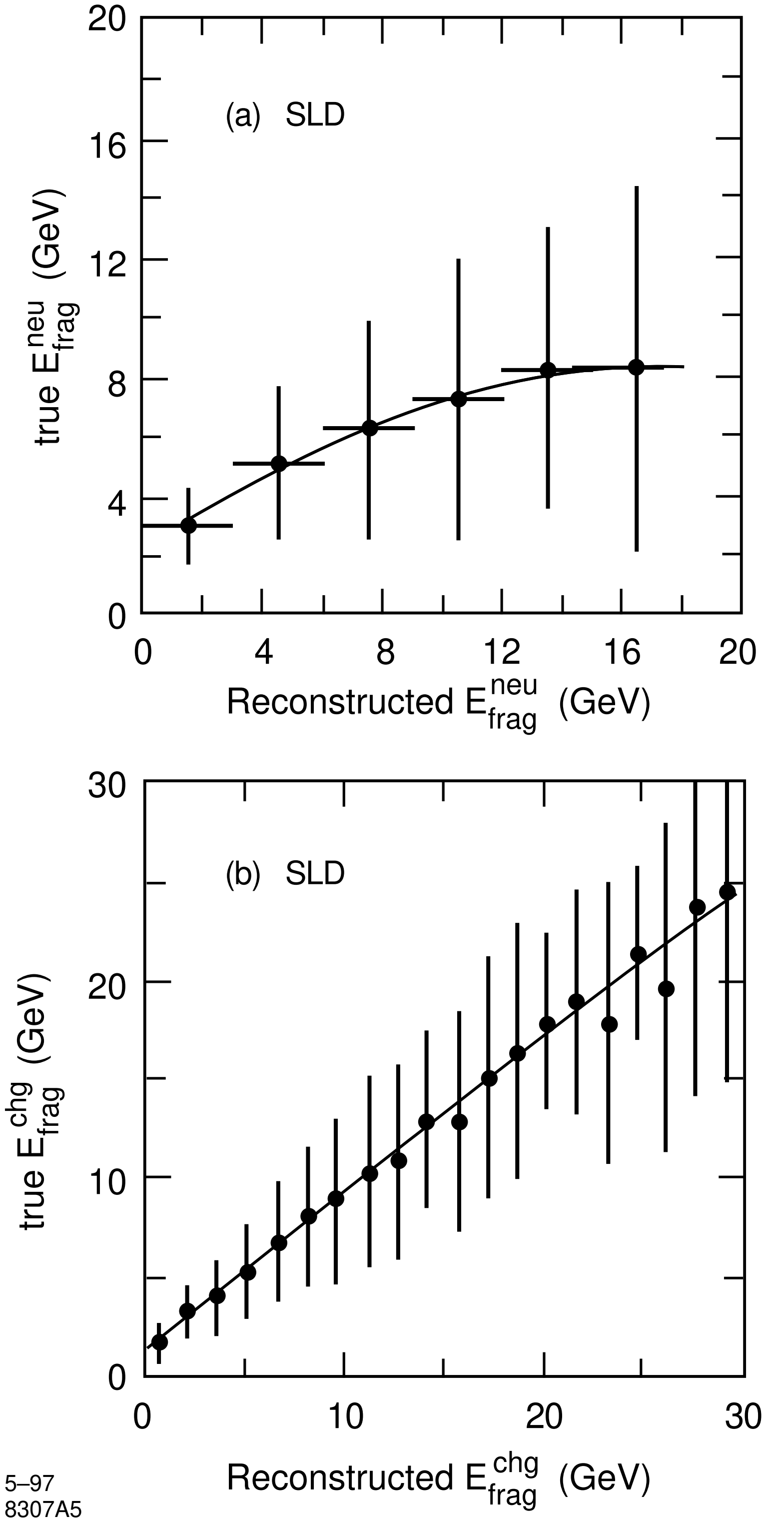

(a) SLD
true E_{frag}^{neu} (GeV)
Reconstructed E_{frag}^{neu} (GeV)
(b) SLD
true E_{frag}^{chg} (GeV)
Reconstructed E_{frag}^{chg} (GeV)
5–97
8307A5

Figure 5:

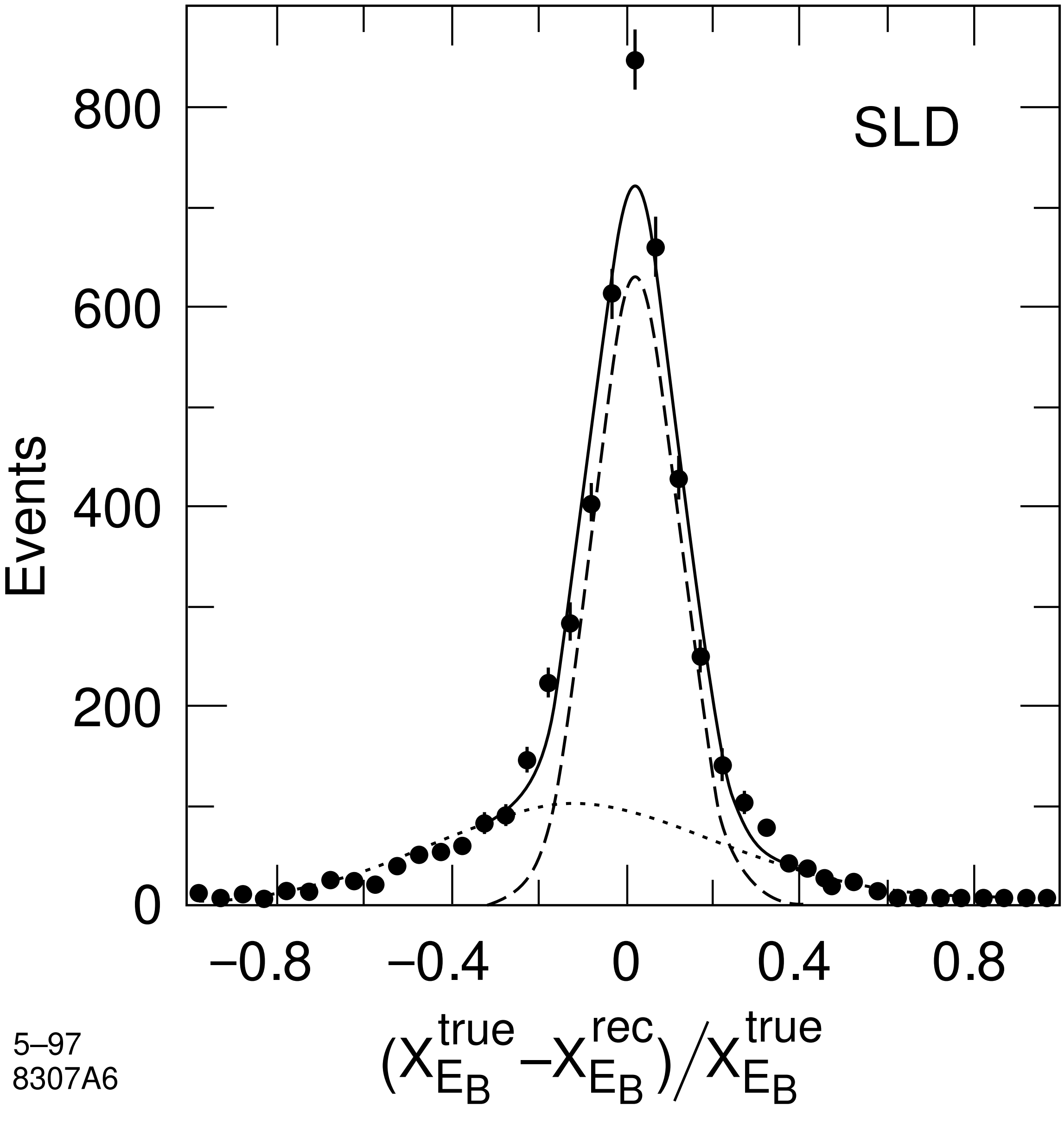
SLD
Events
800
600
400
200
0
−0.8
−0.4
0
0.4
0.8
$(X_{E_B}^{true} - X_{E_B}^{rec})/X_{E_B}^{true}$
5–97
8307A6

Figure 6:

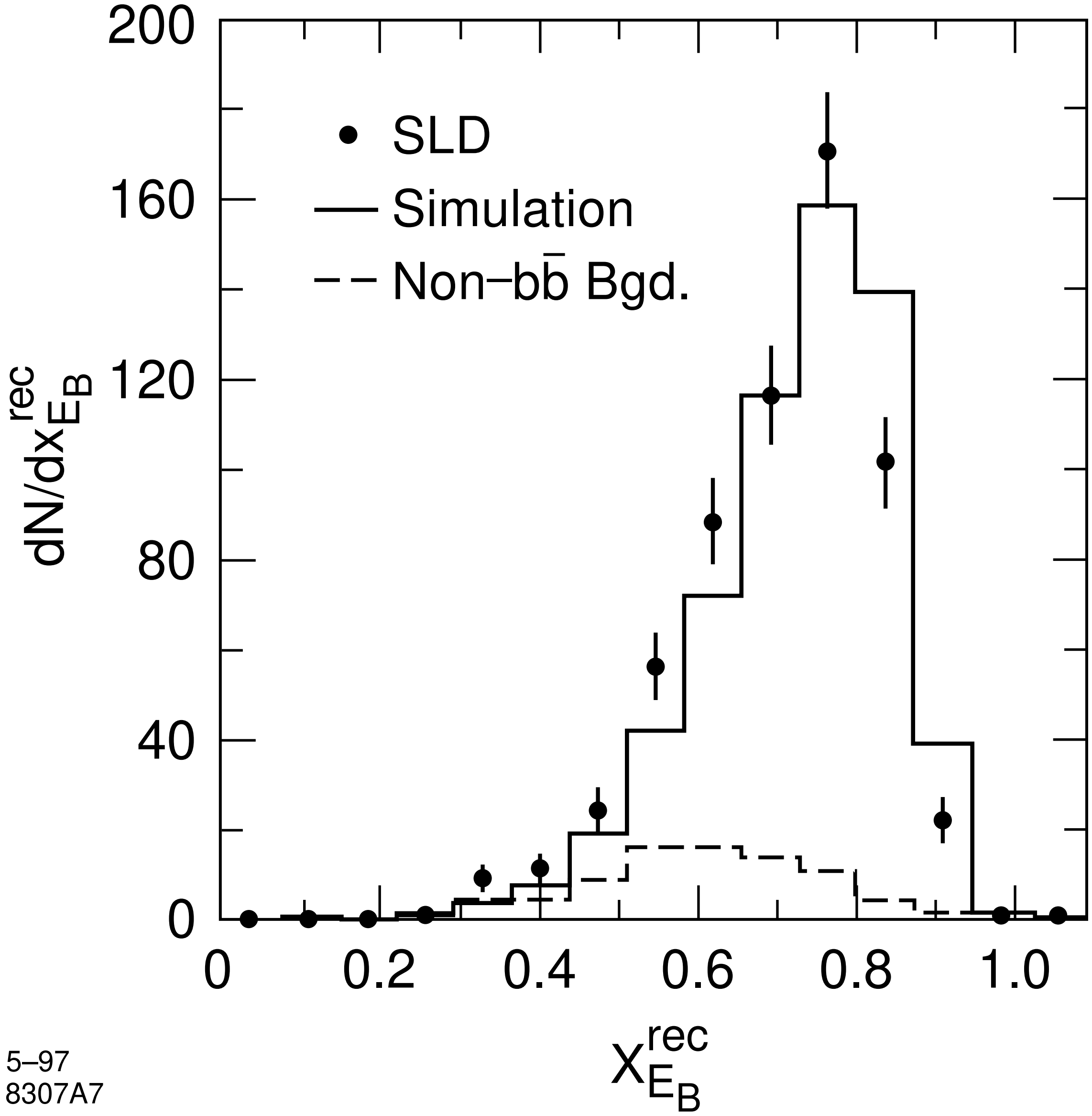

200
160
120
80
40
0
0
0.2
0.4
0.6
0.8
1.0
SLD
Simulation
Non–b$\bar{b}$ Bgd.
$dN/dx^{rec}_{E_B}$
$X^{rec}_{E_B}$
5–97
8307A7

Figure 7:

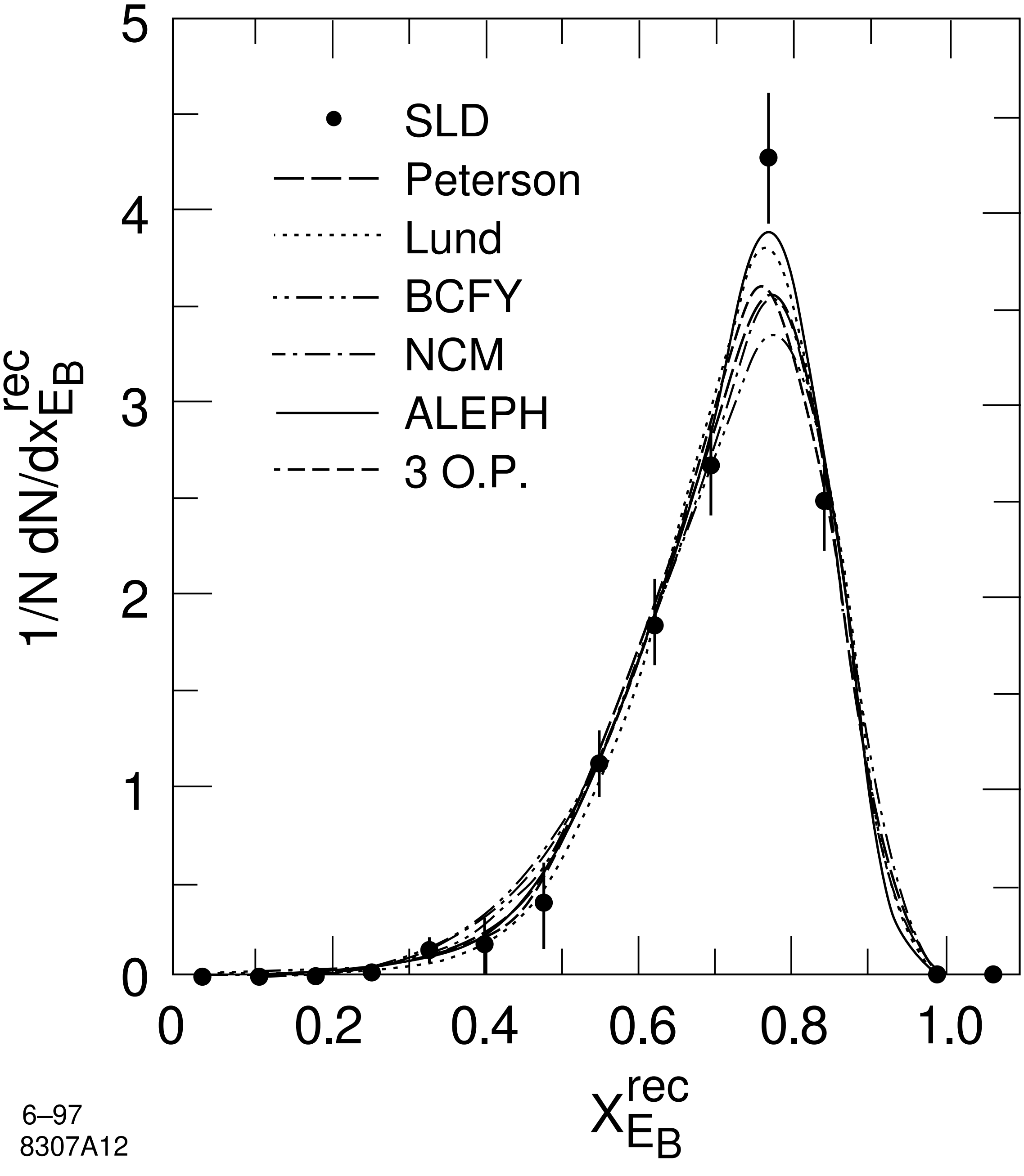
SLD
Peterson
Lund
BCFY
NCM
ALEPH
3 O.P.
$1/N\ dN/dx^{rec}_{E_B}$
$X^{rec}_{E_B}$
0
1
2
3
4
5
0
0.2
0.4
0.6
0.8
1.0
6–97
8307A12

Figure 8:

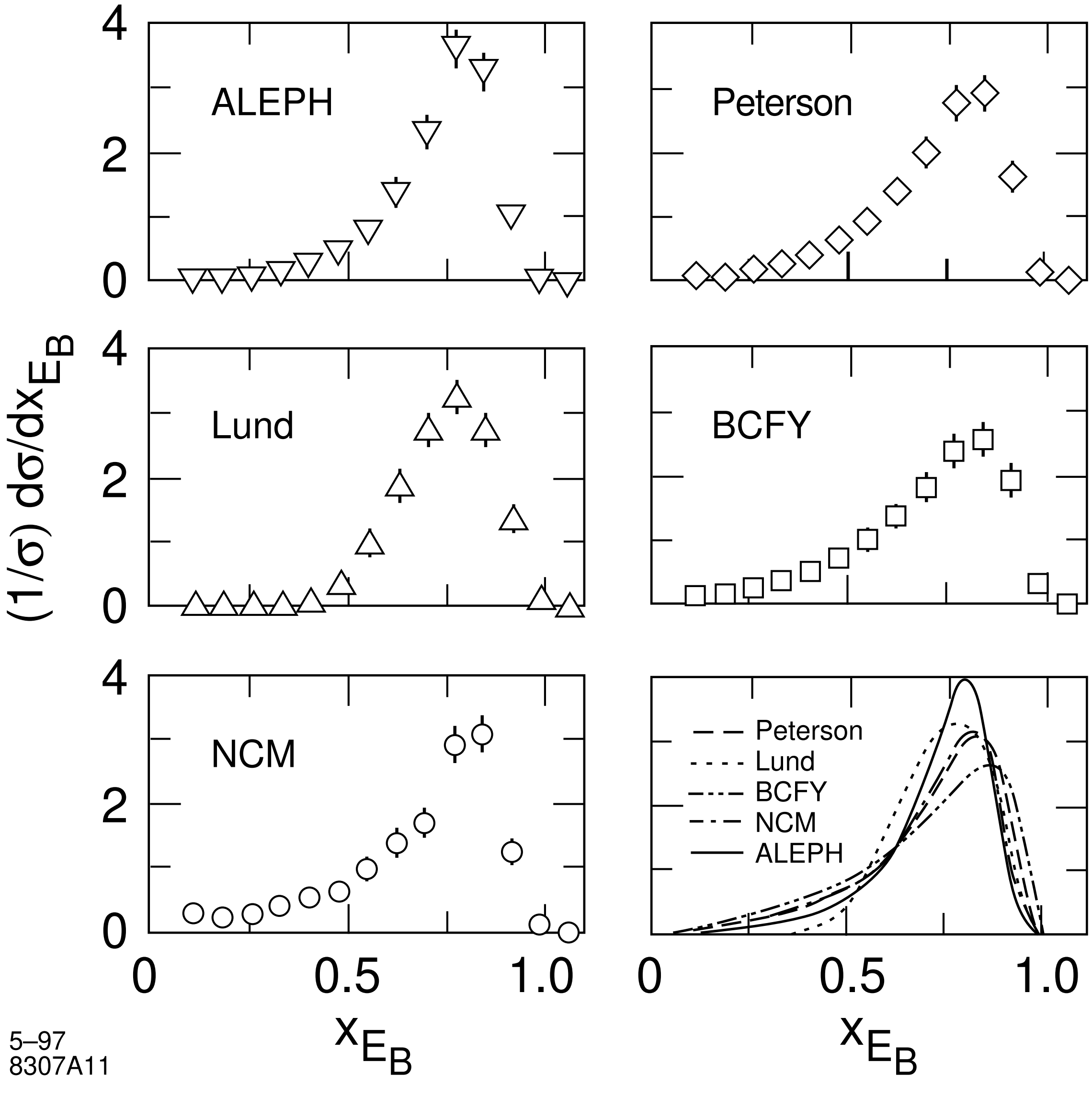
ALEPH
Peterson
Lund
BCFY
NCM
Peterson
Lund
BCFY
NCM
ALEPH
$(1/\sigma)\, d\sigma/dx_{E_B}$
x_{E_B}
x_{E_B}
0
2
4
0
0.5
1.0
5–97
8307A11

Figure 9:

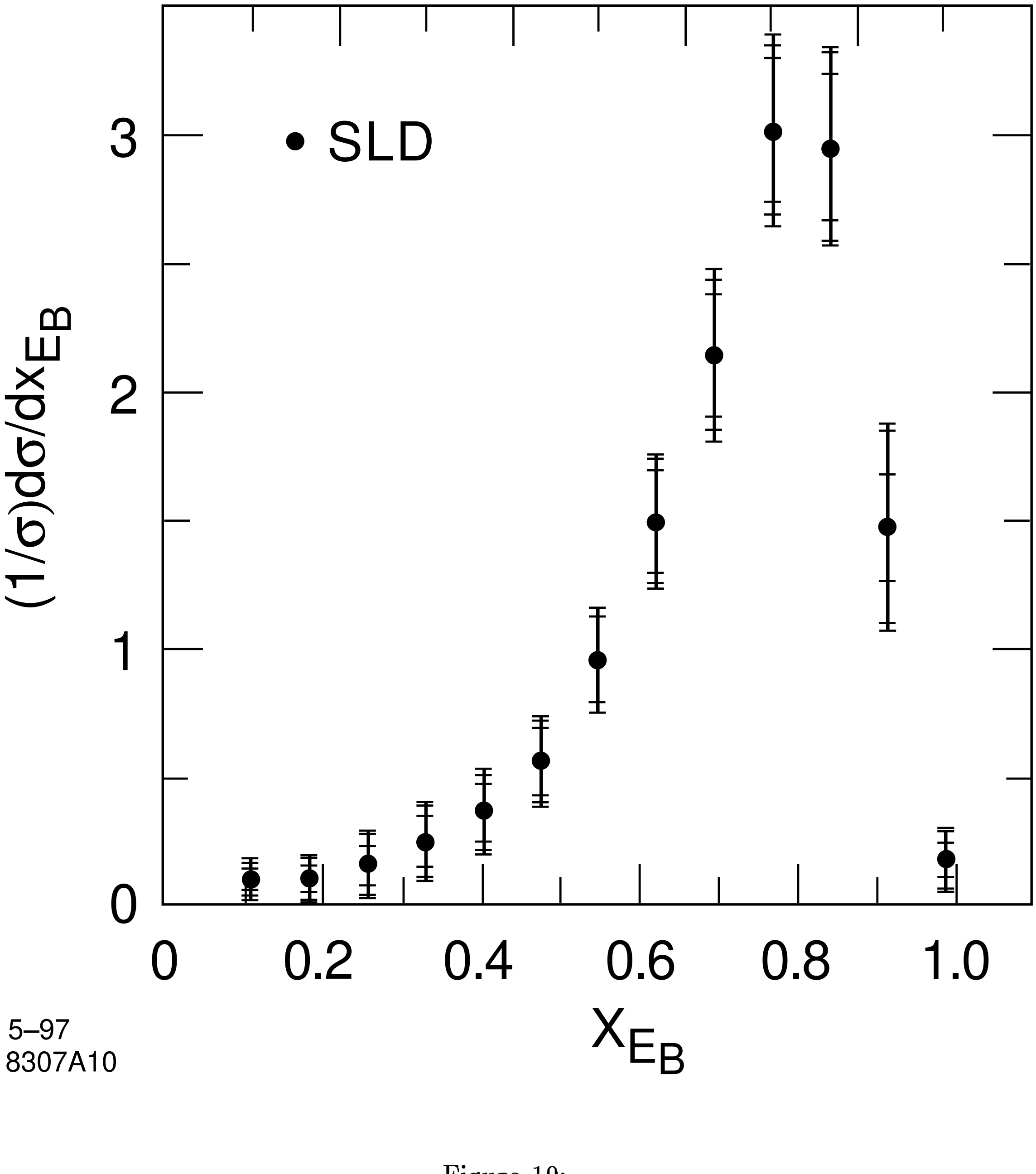

Figure 10: